Chemistry–A European Journal
Research Article
doi.org/10.1002/chem.202500831
Chemistry Europe
European Chemical Societies Publishing
www.chemeurj.org

Multifunctional Organelle-Targeting Probes for Intracellular Imaging and Enhanced Cancer Phototherapy

Weijun Ma,[a, b] Chen Xie,*[a] Xiaomin Li,[a] Leo K. B. Tam,[a] Yue Wu,[a] Rui Wang,[a] Pak-Lun Lam,[a] Ho-Fai Chau,[a] and Ka-Leung Wong*[a]

Photodynamic therapy (PDT) represents a promising modality for cancer treatment; however, its clinical application is hindered by challenges such as glutathione (GSH)-mediated quenching of reactive oxygen species (ROS) and autofluorescence interference during visible light imaging. This study introduces **Cy-NBD-5F**, a photosensitizer engineered to address these limitations. Upon activation by GSH, **Cy-NBD-5F** exhibits 5.5-fold fluorescence enhancement at 701 nm, producing its reduced form, **Cy-OH-5F**, which demonstrates enhanced ROS generation, including a 1.4-fold increase in singlet oxygen and 1.2-fold increase in superoxide anion radicals. Under light irradiation, **Cy-OH-5F** induces significant cytotoxicity (IC_{50} < 3 μM). Additionally, the molecule predominantly localizes within lysosomes and the endoplasmic reticulum, showing organelle-specific effects to improve therapeutic efficacy. These findings show the potential of **Cy-NBD-5F** as a precise and effective tool for cancer theranostics.

1. Introduction

Photodynamic therapy (PDT) has gained significant attention as a cancer treatment,[1] due to its minimally invasive procedure, low toxicity, and repeated application without drug resistance.[2] In normal cells, the oxidative balance is maintained by both the reducing agent glutathione (GSH) and the oxidizing agent reactive oxygen species (ROS), while in cancer cells, this balance is disrupted and GSH is overexpressed to 10 mM, compared to 1–2 mM in most normal cells.[3] This GSH overexpression has been widely used as a biomarker to activate phototheranostic, and some compounds have been reported to moderate the intracellular ROS and GSH levels to achieve therapeutic outcomes.[4] Meanwhile, short-wavelength excitation is not suitable for PDT because of its limited tissue penetration and adverse health effects. The concept of precision medicine, which focuses on maximizing the elimination of tumor tissue while reducing side effects on normal tissue, is widely recognized in the context of exploring effective treatment methods for cancer.[5]

From a microscopic view, organelle- targeted PDT has shown strong appeal due to its unique advantages.[6] The presence of specific targets can prevent photosensitizers from off-target accumulation and ensure accurate delivery to subcellular compartments, thereby reducing damage to normal tissues during therapy,[7] it may also induce immunogenic cell death (ICD).[8] For instance, recent studies have demonstrated that lysosomes can induce ICD through targeted PDT.[9] On the other hand, it is important to note that endoplasmic reticulum (ER) stress is also recognized as a significant signaling pathway that triggers ICD, which makes ER another subcellular target.[10] Nevertheless, the targeting of a single organelle is challenging in terms of achieving the anticipated therapeutic effect. One promising approach involves the simultaneous targeting of multiple subcellular organelles.[11]

To overcome these issues, activatable photosensitizers which can generate superoxide anion radicals ($O_2^{\bullet-}$) and hydroxyl radicals (OH•) in hypoxic tumor environments are designed for biomarker-mediated release of active phototherapeutic moieties while exhibiting fluorescent signals and exerting PDT to destroy tumor cells.[12] Hemicyanines, as a subclass of cyanine dyes, feature the D–π–A-based intramolecular charge transfer (ICT) mechanism, and have been widely applied.[13] Qu et al. linked bromine substituted hemicyanine structures with commercial anticancer drug 50-DFUR through H_2O_2 sensitive diborate ester groups to form anticancer prodrugs.[14] Peng et al. synthesized a tumor activating photosensitizer ICy-N with enhanced PDT effect by modulating the indole segment of hemicyanine dye with iodine atoms.[15] In vivo studies have indicated that ICy-N has potential for utilization in tumor hypoxia imaging and near-infrared (NIR) tumor ablation. Recently, Miao et al. designed and synthesized an APN activatable hemicyanine dye-based phototheranostic probe (CyA), which activates fluorophotoacoustic signal-guided PDT and immunotherapy for effective

[a] W. Ma, Dr. C. Xie, X. Li, Dr. L. K. B. Tam, Dr. Y. Wu, Dr. R. Wang, P.-L. Lam, Dr. H.-F. Chau, Prof. Dr. K.-L. Wong
Department of Applied Biology and Chemical Technology, The Hong Kong Polytechnic University, Hung Hom, Hong Kong Special Administrative Region of China
E-mail: chenxie@polyu.edu.hk
klgwong@polyu.edu.hk

[b] W. Ma
Department of Chemistry, Hong Kong Baptist University, Kowloon Tong, Hong Kong Special Administrative Region of China

Supporting information for this article is available on the WWW under https://doi.org/10.1002/chem.202500831

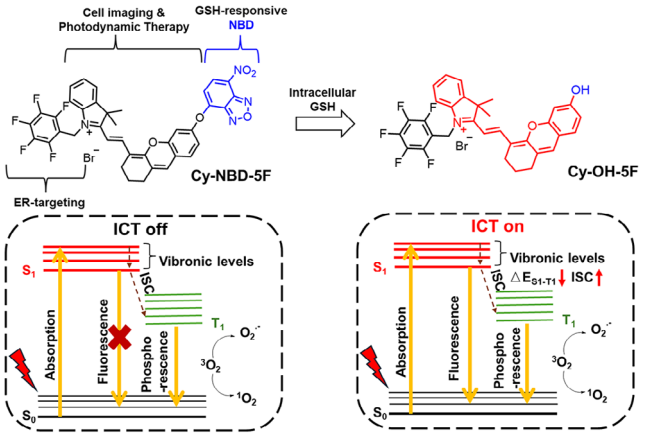

Scheme 1. Molecular structures and proposed mechanism of **Cy-NBD-5F** for GSH-responsive imaging and photodynamic therapy. Upon activation by intracellular GSH, **Cy-NBD-5F** transitions to **Cy-OH-5F**, enabling fluorescence turn-on, enhanced intersystem crossing (ISC), and increased ROS generation.

tumor treatment.[8] These good works provide a foundation for designing and synthesizing new phototheranostic based on hemicyanine dyes, although most organic photosensitizers are designed for "always-on" fluorescencent signal, which can lead to inability to activate biomarkers for therapeutic diagnosis, while the "off-on" property allows for minimal background fluorescence and a high signal-to-noise ratio at tumor sites, so that improving diagnostic precision.[16]

Herein, we designed a small-molecule photosensitizer (**Cy-NBD-5F**) based on the hemicyanine dye, the fluorobenzene moiety for organelle-targeting, and a GSH-activatable functional group (7-nitro-2,1,3-benzoxadiazole, NBD). With GSH overexpression in tumor cells, **Cy-NBD-5F** is reduced to **Cy-OH-5F**, and ICT is restored, thereby producing NIR fluorescence and enhanced inhibitory effects (Scheme 1). The NBD moiety greatly contributes to the enhanced performance in therapeutic treatment, by avoiding the high dark toxicity from **Cy-OH-5F**, increasing the cellular uptake, and moderately enhancing ROS and singlet oxygen production. We have comprehensively evaluated its ROS production ability and responsive signaling, applied the compounds to cells, and demonstrated their promising theranostic applicability.

2. Results and Discussion

2.1. Photophysical Properties

To establish the suitability of **Cy-NBD-5F** for cell imaging and PDT, its photophysical properties were thoroughly investigated. **Cy-NBD-5F** and **Cy-OH-5F** were successfully synthesized with good water solubility (Scheme S1), and their structures were characterized using $^{1}H/^{13}C/^{19}F$ NMR spectroscopy, ESI mass spectrometry, and HPLC. As shown in Figure 1, the maximum absorption peak of **Cy-NBD-5F** is at 597 nm, while **Cy-OH-5F** exhibits a red-shifted absorption peak at 651 nm, which is consistent with its structural changes. While **Cy-NBD-5F** shows weak

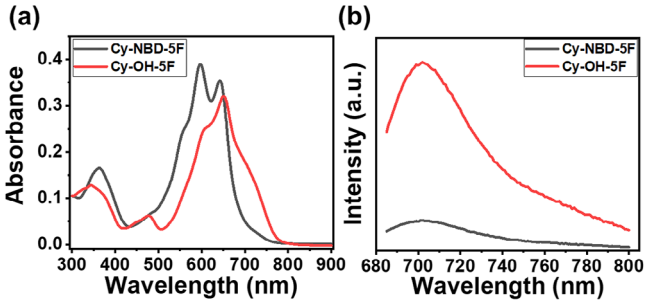

Figure 1. a) UV-Vis absorption spectra and b) fluorescence emission spectra of **Cy-NBD-5F** and **Cy-OH-5F** (10 μM) in PBS buffer (pH 7.4, containing 1% DMSO). Excitation wavelength (λ_{ex}) = 670 nm.

fluorescence in PBS buffer (1% DMSO), its reduced product, **Cy-OH-5F**, emits strong fluorescence at 701 nm (Figure 1b). This turn-on NIR fluorescence is advantageous for tumor imaging, as longer wavelengths enable deeper tissue penetration under light irradiation.[10] The fluorescence quantum yields were measured to be 0.31% for **Cy-NBD-5F** and 0.99% for **Cy-OH-5F** using methylene blue (MB) as the standard (Figures S1–S3 and Table S1).

The GSH levels are often associated with diseases.[17] The time-response profiles of **Cy-NBD-5F** with GSH are shown in Figure 2. Upon GSH treatment, a new absorption band at 651 nm corresponding to **Cy-OH-5F** increases progressively, while the absorption intensity of **Cy-NBD-5F** at 597 nm decreases over time (Figure 2a). Quantitative analysis of the conversion in solution was performed by HPLC, monitoring 10 μM **Cy-NBD-5F** in the presence of 5 mM GSH in PBS buffer. The conversion rate was calculated based on the relative peak areas of the reactant and product. As shown in Figure S4 and Table S2, approximately 90% of **Cy-NBD-5F** was reduced to **Cy-OH-5F** within 4 hours. Simultaneously, the fluorescence intensity at 701 nm increases significantly (Figure 2b), confirming the conversion of **Cy-NBD-5F** to **Cy-OH-5F**. This molecular transformation is facilitated by the donor–π–acceptor (D–π–A) configuration of **Cy-NBD-5F**, where the removal of the NBD group enhances ICT, resulting in stronger fluorescence emission. The structural conversion was further confirmed by ESI-MS analysis, which identified **Cy-OH-5F** (m/z = 550.7) and **Cy-NBD-5F** (m/z = 713.5) as the respective product and the precursor (Figure S5). Additionally, a linear relationship between fluorescence intensity and GSH concentration was obtained in the range of 20–100 μM (Figure 2d), making **Cy-NBD-5F** a reliable probe for detecting abnormal GSH in a practical biological range.

The specificity of **Cy-NBD-5F** toward GSH was evaluated against a panel of potential interfering species, including Cys, Hcy, Lys, Pro, His, Arg, Ser, Glucose, H_2O_2, Ca^{2+}, and Mg^{2+}. As shown in Figure 2e,f, the addition of 1 mM GSH resulted in around 5.5-fold fluorescence enhancement at 701 nm, while negligible responses were observed with the other species, except for bio-thiols Hcy (200 μM) and Cys (200 μM). Although **Cy-NBD-5F** shows reactivity toward homocysteine (Hcy) and cysteine (Cys), the physiological concentrations of these two thiols are significantly lower than that of glutathione (GSH) in biological systems. Typically, GSH exists at concentrations of

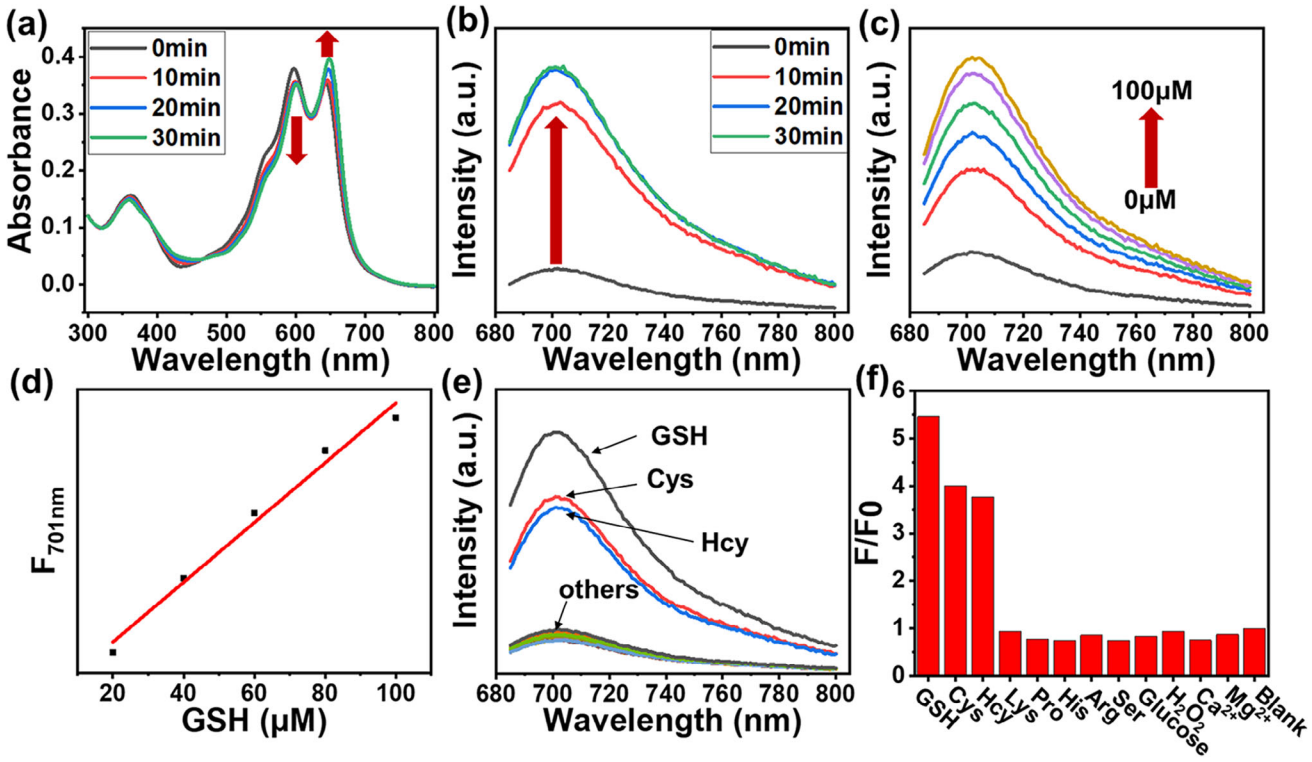

Figure 2. Evolution of **Cy-NBD-5F** (10 μM) to **Cy-OH-5F** upon GSH (5 mM) addition, measured via a) UV-Vis spectra and b) fluorescence spectra in PBS (pH 7.4, 1% DMSO). c) Fluorescence titration of **Cy-NBD-5F** (10 μM) with different GSH concentrations (0, 20, 40, 60, 80, 100 μM). d) Linear correlation between fluorescence intensity at 701 nm and GSH concentration. e) Fluorescence response and f) F/F_n values of **Cy-NBD-5F** (10 μM) in the presence of GSH (1 mM), Cys (200 μM), Hcy (200 μM), and other relevant species (1 mM). λ_{ex} = 670 nm, λ_{em} = 701 nm.

1–10 mM in cancer cells, while Cys and Hcy are present only at 30–200 μM and 5–12 μM, respectively. As a result, the interference from Cys and Hcy is minimal under biological conditions. This selectivity exhibits the potential of **Cy-NBD-5F** for reliable GSH quantification.

2.2. Production of ROS

1,3-Diphenylisobenzofuran (DPBF) was used as a singlet oxygen trapping agent, with MB serving as a reference to evaluate singlet oxygen generation.[15] As shown in Figure 3b, the absorbance of DPBF at 415 nm decreased significantly in the presence of **Cy-OH-5F** under visible-light irradiation, whereas **Cy-NBD-5F** induced only weak DPBF bleaching under identical conditions (Figure 3a). The singlet oxygen quantum yields (Φ_Δ) were calculated as 2.20% for **Cy-NBD-5F** and 3.14% for **Cy-OH-5F**, suggesting that the removal of the NBD group enhances the ability to generate singlet oxygen (Figure 3c). This enhanced singlet oxygen generation ability of **Cy-OH-5F** is promising and stronger than some reported photosensitizers.[15] This finding is consistent with the hypothesis that the NBD group suppresses the electron-donating capacity of hydroxyl groups, thereby limiting ICT and reducing singlet oxygen production. This ROS production was further validated using Singlet Oxygen Sensor Green (SOSG), a highly selective probe for emitting strong green fluorescence after reacting with singlet oxygen.[18] As shown in Figure S6, no significant change in fluorescence intensity was observed in the **Cy-NBD-5F** and SOSG mixture before and after light irradiation, but after the reaction with GSH, the significantly enhanced emission from SOSG can be seen to prove the increase singlet oxygen production.

To explore their Type-I PDT ability, exhibited by superoxide anion radical ($O_2^{\bullet-}$) generation capacity, we used the fluorescent probe dihydrorhodamine 123 (DHR123) and the reductant vitamin (Vc) as indicators.[19] As shown in Figure 3d–3f, DHR123 which was nonfluorescent but can react with ROS, generated from both **Cy-NBD-5F** and **Cy-OH-5F** via Type I PDT process, to emit strong green fluorescence centered at 533 nm. After the addition of Vc, **Cy-OH-5F** showed much reduced emission intensity which further validates that the enhanced DHR123 signal was indeed caused by generated ROS. These results indicate that both compounds can generate singlet oxygen and superoxide anion radicals, but their ROS generation efficiency improves after GSH-mediated conversion of **Cy-NBD-5F** to **Cy-OH-5F**. By evaluating the production of different types of ROS, the reduced product **Cy-OH-5F** exhibited about 1.4-fold increase in singlet oxygen generation and around 1.2-fold increase in superoxide anion radical production compared to **Cy-NBD-5F**.

Considering the difference of matrix/solvent polarities in complex biological condition. The fluorescence properties of **Cy-NBD-5F** and **Cy-OH-5F** were also evaluated in relation to solution polarity. As polarity decreased, fluorescence intensity increased

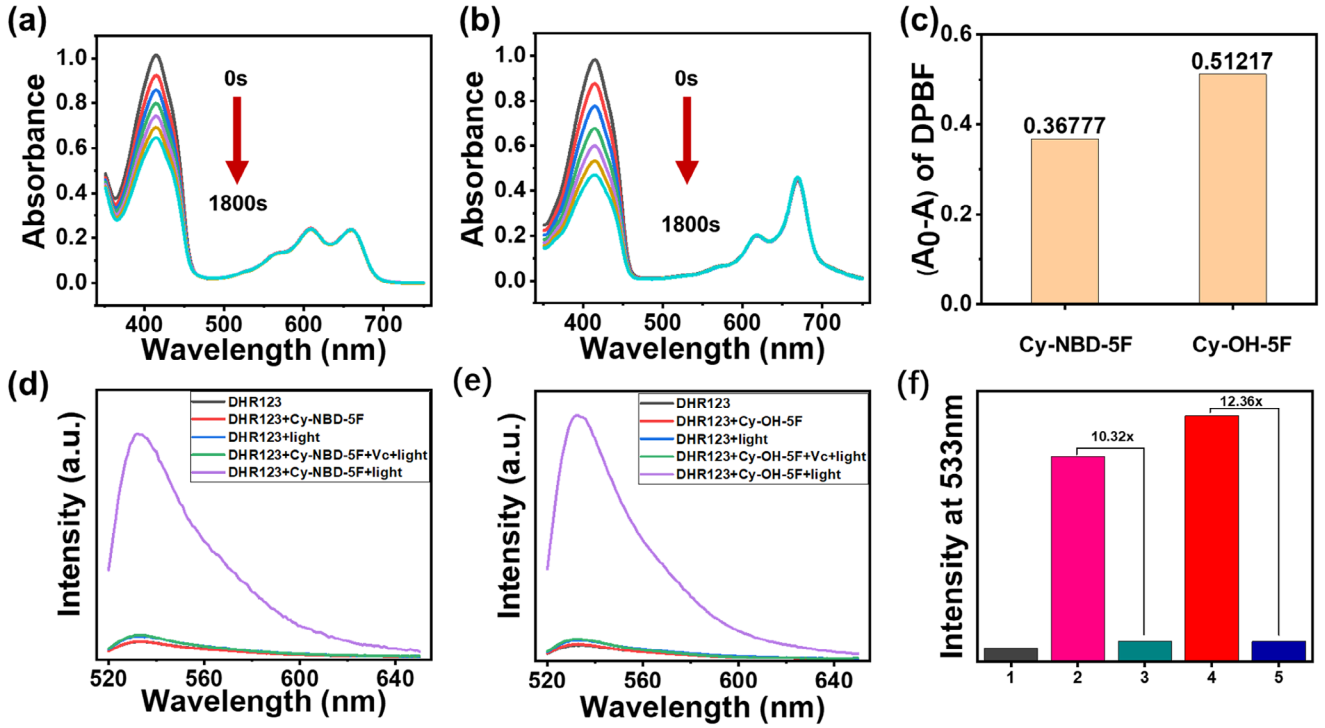

Figure 3. Photodegradation curves of DPBF (120 μM) induced by ROS from a) **Cy-NBD-5F** (5 μM) and b) **Cy-OH-5F** (5 μM) in DCM under visible-light irradiation. c) Decrease in DPBF absorbance at 415 nm. Fluorescence spectra of DHR123 (10 μM) with d) **Cy-NBD-5F** (10 μM) and e) **Cy-OH-5F** (10 μM) and Vc (50 μM) under visible-light irradiation for 5 minutes in aqueous solution (1% DMSO). f) Fluorescence intensity of DHR123 at 533 nm after visible-light irradiation for 5 minutes (1: DHR123; 2: DHR123 + **Cy-NBD-5F** + light; 3: DHR123 + **Cy-NBD-5F** + Vc + light; 4: DHR123 + **Cy-OH-5F** + light; 5: DHR123 + **Cy-OH-5F** + Vc + light).

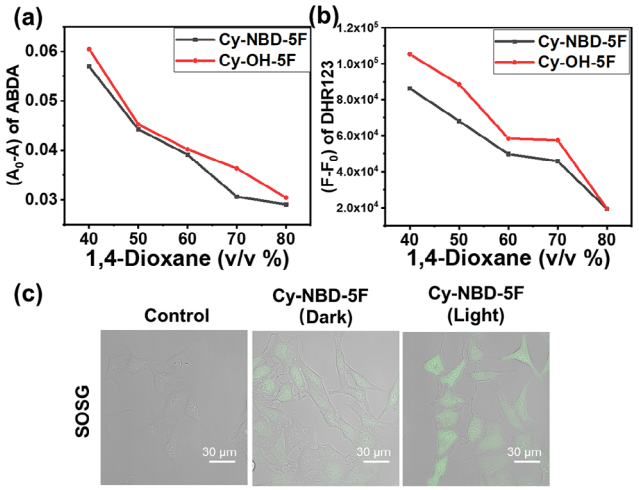

Figure 4. a) Polarity-dependent absorbance of ABDA (100 μM) with **Cy-NBD-5F** (10 μM) and **Cy-OH-5F** (10 μM) at 378 nm in mixtures of 1,4-dioxane and water (*v/v*%). b) Polarity-dependent fluorescence intensity of DHR123 (10 μM) with **Cy-NBD-5F** (10 μM) and **Cy-OH-5F** (10 μM) at 533 nm in 1,4-dioxane/water solutions (*v/v*%). c) The fluorescence imaging of the HeLa cells incubated with **Cy-NBD-5F** (2.5 μM) activated by GSH. SOSG fluorescence indicates ROS generation under red LED irradiation (5 J) after 20-hour of incubation. Scale bar = 30 μm.

(Figure S7), highlighting their sensitivity to environmental polarity changes. This characteristic suggests potential applications in monitoring organelle polarity, such as changes in the ER during ferroptosis.[20] However, the ability to generate singlet oxygen (Figures 4a and S8,S9) and superoxide anion radicals (Figures 4b, and S10, S11) decreased with reduced polarity. This behavior is attributed to the reduced singlet-triplet energy gap ($\Delta E_{S,T}$) in polar environments, which facilitates intersystem crossing (ISC) and enhances ROS generation.[21]

2.3. In Vitro Cell Imaging and Photodynamic Therapeutic Effects

To further assess the applicability of **Cy-NBD-5F**, its intracellular ROS generation ability was evaluated in HeLa cells following GSH activation. SOSG was employed as an indicator, as it reacts with ROS to emit a fluorescent signal. HeLa cells were incubated with **Cy-NBD-5F** for 20 hours, followed by two control experiments: one group was irradiated with a red LED light (5 J), while the other group was kept in the dark. Noteworthily, red-light irradiation is preferred in biological studies due to its superior tissue penetration and reduced photodamage. As shown in Figure 4c, cells incubated with **Cy-NBD-5F** and exposed to light exhibited a strong fluorescent green signal, whereas the dark control group displayed only weak fluorescence. This weak fluorescent signal could be attributed to the reaction between endogenous ROS and the probe, because ROS are naturally produced in normal cellular metabolism and are abundant in organelles such as mitochondria, peroxisomes, and the ER.[22] These results indicate that **Cy-NBD-5F**, after GSH activation, generates ROS efficiently under light irradiation. This controllable activation minimizes toxic side effects on normal cells.

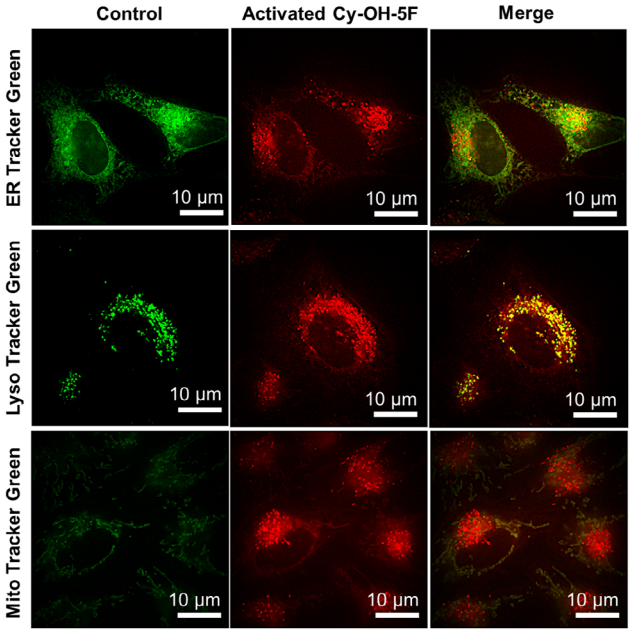

Figure 5. a) Confocal laser scanning microscopy (CLSM) images of HeLa cells incubated with **Cy-NBD-5F** (2 μM) for 16 hours, showing colocalization with organelle-specific dyes for the endoplasmic reticulum (ER Tracker Green), lysosomes (Lyso Tracker Green), and mitochondria (Mito Tracker Green). λ_{ex} = 638 nm. Scale bar = 10 μm.

The subcellular localization of **Cy-NBD-5F** in HeLa cells was investigated using confocal laser scanning microscopy (CLSM). Commercial organelle-staining trackers, including mitochondria (Mito)-Tracker Green, lysosome (Lyso)-Tracker Green, and endoplasmic reticulum (ER)-Tracker Green, were employed. As shown in Figure 5, **Cy-NBD-5F** preferentially localizes in the ER and lysosomes after GSH activation. Costaining with ER-Tracker Green yielded a Pearson's correlation coefficient of 0.65, confirming ER targeting. This targeting is likely attributed to the polyfluorophenyl group of **Cy-NBD-5F**, which enhances its hydrophobicity and promotes interaction with the hydrophobic regions of the ER.[23] Similarly, colocalization with Lyso-Tracker Green yielded a Pearson's correlation coefficient of 0.73, indicating lysosomal localization. This lysosomal targeting facilitates the generation of ROS under light irradiation, leading to lysosomal rupture and subsequent apoptosis through the release of photosensitizers into the cytoplasm.[24] Further CLSM analysis revealed that few yellow pixels were observed in the merged images of **Cy-NBD-5F** with Mito-Tracker Green, yielding a Pearson's correlation coefficient below 0.26. This indicates that **Cy-NBD-5F** activated by GSH does not localize in mitochondria. The dual localization of **Cy-NBD-5F** in the ER and lysosomes highlights its potential to induce ICD by generating ROS and triggering ER stress, a promising strategy for photoimmunotherapy.[25]

The photodynamic therapeutic efficacy of the precursor **Cy-NBD-5F** and its active drug **Cy-OH-5F** was evaluated using an MTT assay in HeLa cells (cervical cancer cells), HTB-9 cells (bladder cancer cells), MRC-5 cells (normal lung cells), and L-02 cells (normal liver cells). After 24 hours of incubation, **Cy-OH-5F** demonstrated higher inhibitory activities to all cell lines even under dark conditions, compared to **Cy-NBD-5F** (Figure 6,

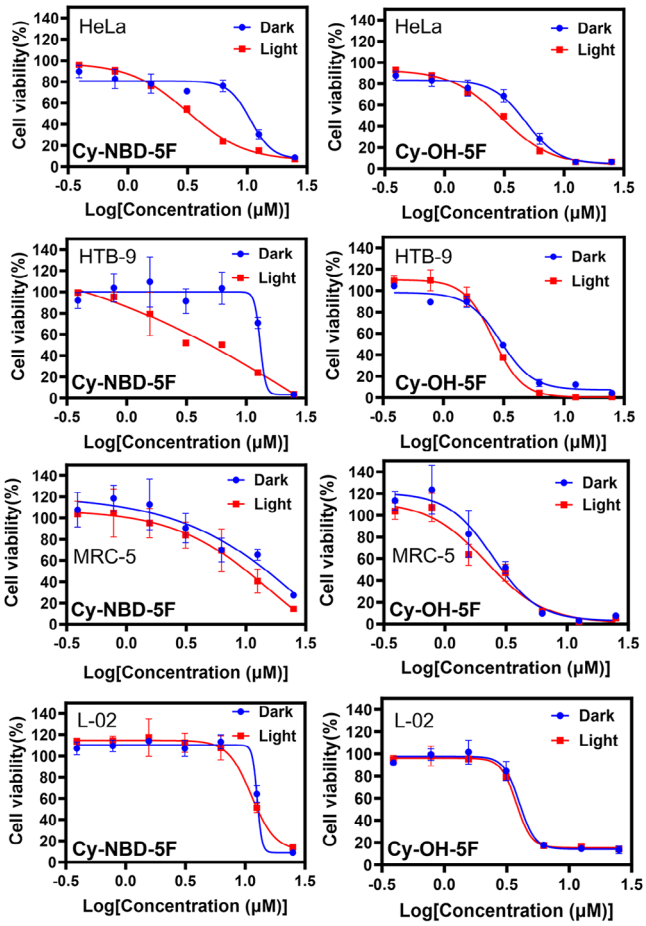

Figure 6. Cytotoxicity of **Cy-NBD-5F** and **Cy-OH-5F** under dark conditions and upon irradiation with red light (635 nm, 0.5 J) at various concentrations in different cell lines. Cell viability (%) is plotted against the logarithm of compound concentration.

Table 1. IC_{5n} values (μM) of different cells treated with **Cy-NBD-5F** and **Cy-OH-5F**, under dark conditions and upon irradiation with red light (635 nm, 0.5 J).

		Cy-NBD-5F	Cy-OH-5F
HeLa	*Dark*	10.64	4.78
	Light	3.16	2.98
HTB-9	*Dark*	13.33	2.96
	Light	6.54	2.66
MRC-5	*Dark*	14.50	2.47
	Light	12.07	2.19
L-02	*Dark*	12.78	3.96
	Light	11.48	3.67

Table 1). The different dark IC_{50} values between the two samples suggest that the conversion of **Cy-NBD-5F** to **Cy-OH-5F** was partial, which might be due to the subcellular localization GSH. It has been reported that, compared to cytosol and mitochondria, much less GSH residues in the ER or lysosomes (where our compounds localize),[26] leading to reduced local availability for prodrug activation.

Under red light irradiation (635 nm, 0.5 J), **Cy-NBD-5F** showed a increase in phototoxicity, with its IC_{50} of 3.16 μM in HeLa cells, close to that of **Cy-OH-5F** (2.98 μM). This supports the occurrence of intracellular conversion. In HTB-9 cells, a similar trend was observed. **Cy-NBD-5F** also demonstrated substantial light-induced cytotoxicity (IC_{50} = 6.54 μM), indicating effective PDT potential in this cancer cell line. Although the phototoxicity was higher for **Cy-OH-5F** (2.66 μM), the GSH&light-induced toxicity enhancement still reflects a therapeutically response to red light irradiation in cancer cells. In contrast, in MRC-5 normal cells, **Cy-NBD-5F** maintained high IC_{50} values under both dark (14.50 μM) and light (12.07 μM) conditions, similar observation in L-02 normal cells, demonstrating minimal conversion and excellent biocompatibility, due to the lower intracellular GSH levels in non-cancerous cells. Besides, Flow cytometry analysis of intracellular compound levels revealed more efficient cellular uptake of **Cy-NBD-5F**, as **Cy-OH-5F** had not fully entered the cells within 12 hours (Figures S12,S13, Table S3).

These results emphasize that the photodynamic therapeutic activity of **Cy-NBD-5F** is dependent on its selective intracellular activation, which varies between cell types. The combination of low dark toxicity, efficient light-triggered cytotoxicity in cancer cells, and high safety in normal cells show the promise of **Cy-NBD-5F** as a tumor-targeted pro-photosensitizer for PDT.

3. Conclusion

In summary, this study presents the design and synthesis of Cy-NBD-5F, a NIR-emitting photosensitizer with promising applications in cancer imaging and PDT. Cy-NBD-5F exhibits weak fluorescence and modest ROS generation in its initial form; however, upon reduction by overexpressed GSH in cancer cells, its reduced product Cy-OH-5F demonstrates a 5.46-fold fluorescence enhancement at 701 nm, along with a 1.4-fold and 1.2-fold increase in singlet oxygen and superoxide anion radical generation, respectively. Additionally, Cy-NBD-5F enables effective monitoring of GSH concentration, with fluorescence intensity showing a strong linear correlation with GSH levels in the 20∼100 μM range. The molecular design, based on ICT enhancement through NBD removal, was validated through polarity-dependent fluorescence and ROS generation studies. Despite polarity changes, Cy-OH-5F consistently outperformed its precursor Cy-NBD-5F in ROS production and fluorescence intensity. Furthermore, the dual-organelle-targeting ability of Cy-NBD-5F, specifically to lysosomes and the ER, underscores its potential for inducing ICD and advancing photoimmunotherapy strategies.[9,10]

Acknowledgments

K.-L. W. gratefully acknowledges the financial assistance from the Hong Kong Research Grants Council Grant No. 12300021, and NSFC/RGC Joint Research Scheme (N_PolyU209/21).

Conflict of Interest

The authors declare no conflict of interest.

Data Availability Statement

The data that support the findings of this study are available on request from the corresponding author. The data are not publicly available due to privacy or ethical restrictions.

Keywords: activatable fluorescence · dual-targeting · hemicyanine dye · nir emission · photodynamic therapy

[1] a) B. Moy, R. B. Rumble, L. A. Carey, *J. Clin. Oncol.* **2023**, *41*, 6; b) L. R. H. Gerken, M. E. Gerdes, M. Pruschy, I. K. Herrmann, *Mater. Horiz.* **2023**,*10*, 4059; c) L. F. Yang, Y. Q. Liu, X. R. Ren, R. X. Jia, L. L. Si, J. S. Bao, Y. Y. Shi, J. J. Sun, Y. Zhong, P. C. Duan, X. Y. Yang, R. Zhu, Y. Jia, F. Bai, *ACS Nano* **2024**, *18*, 3161; d) K. Cullion, C. A. Ostertag-Hill, M. Pan, B. Timko, E. Boscolo, D. S. Kohane, *Nano Lett.* **2023**, *23*, 7092; e) Q. C. Tang, F. Y. Zhang, L. C. Luo, Y. L. Duan, T. M. Zhu, Y. Q. Ni, Y. Wang, H. N. Qi, S. T. Jiang, J. X. Zhou, X. X. Ma, Y. F. Zhang, *ACS Appl. Mater. Interfaces* **2023**, *15*, 50926.

[2] M. Dirak, C. M. Yenici, S. Kolemen, *Coord. Chem. Rev.* **2024**, *506*, 215710.

[3] a) A. Meister, *J. Biol. Chem.* **1988**, *263*, 17205; b) C. V. Smith, D. P. Jones, T. M. Guenthner, L. H. Lash, B. H. Lauterburg, *Toxicol. Appl. Pharmacol.* **1996**, *140*, 1; c) H. J. Forman, H. Zhang, A. Rinna, *Mol. Asp. Med.* **2008**, *30*, 1; d) A. L. Ortega, S. Mena, J. M. Estrela, *Cancers (Basel)* **2011**, *3*, 1285.

[4] a) X. Y. Zhong, X. W. Wang, L. Cheng, Y. A. Tang, G. T. Zhan, F. Gong, R. Zhang, J. Hu, Z. Liu, X. L. Yang, *Adv. Funct. Mater.* **2020**, *30*, 1907954; b) L. Wang, Y. T. Xu, C. Liu, W. L. Si, W. J. Wang, Y. W. Zhang, L. P. Zhong, X. C. Dong, Y. X. Zhao, *Chem. Eng. J.* **2022**, *438*, 135567; c) Z. T. Zhang, R. Y. Wang, X. X. Huang, R. J. Luo, J. W. Xue, J. Gao, W. Y. Liu, F. L. Liu, F. Feng, W. Qu, *ACS Appl. Mater. Interfaces* **2020**, *12*, 5680; d) J. S. Lan, L. Liu, R. F. Zeng, Y. H. Qin, J. W. Hou, S. S. Xie, S. Yue, J. Yang, R. J. Y. Ho, Y. Ding, T. Zhang, *Chem. Eng. J.* **2021**, *407*,127212.

[5] J. Mateo, L. Steuten, P. Aftimos, F. André, M. Davies, E. Garralda, J. Geissler, D. Husereau, I. Martinez-Lopez, N. Normanno, *Nat. Med.* **2022**, *28*, 658.

[6] Q. C. Xiao, H. R. Lin, J. Wu, X. Pang, Q. M. Zhou, Y. Jiang, P. Wang, W. N. Leung, H. K. Lee, S. Jiang, S. Q. Yao, L. Q. Gao, G. Liu, C. S. Xu, *J. Med. Chem.* **2020**, *63*, 4896.

[7] L. H. Zhou, F. F. Wei, J. J. Xiang, H. F. Li, C. B. Li, P. F. Zhang, C. J. Liu, P. Gong, L. T. Cai, K. M. C. Wong, *Chem. Sci.* **2020**, *11*, 12212.

[8] M. Zhao, Y. Y. Zhang, J. Miao, H. Zhou, Y. Jiang, Y. Zhang, M. Q. Miao, W. Chen, W. Xing, Q. Li, Q. Q. Miao, *Adv. Mater.* **2023**, *36*, e2305243.

[9] L. Tu, C. L. Li, Q. H. Ding, A. Sharma, M. Q. Li, J. R. Li, J. S. Kim, Y. Sun, *J. Am. Chem. Soc.* **2024**, *146*, 8991.

[10] M. Dirak, A. Saymaz, A. Acari, Y. Akkoç, H. S. Kocak, C. Yenici, D. Gozuacik, H. Gunduz, S. Kolemen, *Mater. Chem. Front.* **2025**, *9*, 648.

[11] a) W. H. Wang, Y. T. Zhang, Z. S. Wang, X. P. Liu, S. Y. Lu, X. L. Hu, *ACS Nano* **2023**, *17*, 11023–11038; b) T. K. Luo, Y. J. Fan, J. M. Mao, X. M. Jiang, L. Albano, E. Yuan, T. Germanas, W. B. Lin, *Angew. Chem. Int. Ed.* **2023**, *62*, e202301910.

[12] J. Sun, X. Cai, C. Wang, K. Du, W. Chen, F. Feng, S. Wang, *J. Am. Chem. Soc.* **2021**, *143*, 868.

[13] a) W. Sun, S. Guo, C. Hu, J. Fan, X. Peng, *Chem. Rev.* **2016**, *116*, 7768; b) X. Z. Zhao, J. P. Liu, J. L. Fan, H. Chao, X. J. Peng, *Chem. Soc. Rev.* **2021**, *50*, 4185.

[14] H. Liu, X. Hu, K. Li, Y. Liu, Q. Rong, L. Zhu, L. Yuan, F. Qu, X. Zhang, W. Tan, *Chem. Sci.* **2017**, *8*, 7689.

[15] F. Xu, H. D. Li, Q. H. Yao, H. Y. Ge, J. L. Fan, W. Sun, J. Y. Wang, X. J. Peng, *Chem. Sci.* **2019**, *10*, 10586.

[16] a) J. Wang, Y. Hou, W. Lei, Q. Zhou, C. Li, B. Zhang, X. Wang, *ChemPhysChem* **2012**, *13*, 2739; b) Z. P. Zhang, P. Y. Chen, Y. Sun, *Molecules* **2023**, *28*, 5360.

[17] S. M. Feng, S. Y. Gong, Z. P. Zheng, G. Q. Feng, *SENS. ACTUAT B-CHEM* **2022**, *351*, 130940.
[18] Q. Wan, R. Y. Zhang, Z. Y. Zhuang, Y. X. Li, Y. H. Huang, Z. M. Wang, W. J. Zhang, J. Q. Hou, B. Z. Tang, *Adv. Funct. Mater.* **2020**, 2002057.
[19] M. Li, J. Xia, R. Tian, J. Wang, J. Fan, J. Du, S. Long, X. Song, J. W. Foley, X. Peng, *J. Am. Chem. Soc.* **2018**, *140*, 14851.
[20] a) L. Jiang, R. Lan, T. Huang, C.-F. Chan, H. Li, S. Lear, J. Zong, W.-Y. Wong, M. Muk-Lan Lee, B. Dow Chan, W.-L. Chan, W.-S. Lo, N.-K. Mak, M. Li Lung, H. Lok Lung, S.W. Tsao, G. S. Taylor, Z.-X. Bian, W. C. S. Tai, G.-L. Law, W.-T. Wong, S. L. Cobb, K.-L. Wong, *Nat. Biomed. Eng.* **2017**, *1*, 42; b) J. Y. Hu, Y. Q. Sun, X. Geng, J. L. Wang, Y. F. Guo, L. B. Qu, K. Zhang, Z. H. Li, *LIGHT-SCI APPL* **2022**, *11*, 185; c) B. L. Dong, Y. Wang, H. Wei, X. Q. Kong, S. J. Li, T. Yue, *Anal. Chim. Acta* **2023**, *1275*, 341571.
[21] H. Su, K. Hu, W. H. Huang, T. Wang, X. L. Zhang, B. Chen, H. Miao, X. P. Zhang, G. Q. Zhang, *Angew. Chem. Int. Ed.* **2023**, *62*, e202218712.
[22] R. Kumari, D. S. Dkhar, S. Mahapatra, R. K. Divya , P. Chandra, *Microchem. J.* **2022**, *180*, 107615.
[23] D. I. Danylchuk, P. H. Jouard, A. S. Klymchenko, *J. Am. Chem. Soc.* **2021**, *143*, 912–924.
[24] a) Z. Li, J. H. Zou, X. Y. Chen, *Adv. Mater.* **2023**, *35*, 2209529; b) X. H. Liu, D. Y. Fan, Y. M. Ren, S. Huang, J. P. Ding, M. Liu, S. V. Wegner, J. Hou, P. F. Rong, F. Chen, W. B. Zeng, *ACS Appl. Mater. Interfaces* **2023**, *15*, 711.
[25] a) Z. Z. Miao, J. S. Li, S. Zeng, Y. H. Lv, S. R. Jia, D. Ding, W. Li, Q. Liu, *ACS Appl. Mater. Interfaces* **2024**, *16*, 245; b) A. Goujon, A. Colom, K. Straková, V. Mercier, D. Mahecic, S. Manley, N. Sakai, A. Roux, S. Matile, *J. Am. Chem. Soc.* **2019**, *141*, 3380–3384.
[26] S. C. Lu, *Biochim. Biophys. Acta* **2013**, *1830*, 3143.

Manuscript received: March 3, 2025
Revised manuscript received: June 3, 2025
Version of record online: June 18, 2025